Indirect CP violation in the neutral kaon system beyond leading logarithms

Stefan Herrlich*
Paul Scherrer Institut, CH-5232 Villigen PSI, Switzerland

Ulrich Nierste†
Physik-Department, TU München, D-85747 Garching, Germany
(Received 10 July 1995)

We have calculated the short distance QCD coefficient η_3 of the effective $|\Delta S|=2$ Hamiltonian in the next-to-leading order of renormalization-group improved perturbation theory. Since now all coefficients η_1, η_2, and η_3 are known beyond the leading log approximation, one can achieve a much higher precision in the theoretical analysis of ε_K, the parameter of indirect CP violation in K^0-$\overline{K^0}$-mixing. The measured value for ε_K yields a lower bound on each of $|V_{cb}|$, $|V_{ub}/V_{cb}|$, the top quark mass m_t, and the nonperturbative parameter B_K as a function of the remaining three quantities. For example, $m_t^{\rm pole}=176$ GeV, $|V_{cb}|=0.040$, and $B_K=0.75$ implies $|V_{ub}/V_{cb}|\geq 0.0778$, if the measured value for ε_K is attributed solely to standard model physics. We further discuss the implications on the CKM phase δ, $|V_{td}|$, and the key quantity for all CP-violating processes, $\mathrm{Im}\,\lambda_t=\mathrm{Im}\,[V_{ts}^*V_{td}]$. These quantities and the improved Wolfenstein parameters $\bar\rho$ and $\bar\eta$ are tabulated and the shape of the unitarity triangle is discussed. We compare the range for $|V_{td}|$ with the one obtained from the analysis of B_d^0-$\overline{B}_d^0$-mixing. For $0.037\leq|V_{cb}|\leq 0.043$, $0.06\leq|V_{ub}/V_{cb}|\leq 0.10$, and $0.65\leq B_K\leq 0.85$ we find from a combined analysis of ε_K and the B_d^0-$\overline{B}_d^0$-mixing paramater x_d: $49^\circ\leq\delta\leq 146^\circ$, $7.4\times10^{-3}\leq|V_{td}|\leq 12.4\times10^{-3}$, $0.85\times10^{-4}\leq\mathrm{Im}\,\lambda_t\leq 1.60\times10^{-4}$, $-0.36\leq\bar\rho\leq 0.28$, and $0.21\leq\bar\eta\leq 0.44$. We predict the mass difference of the B_s^0 system to lie in the range $6.5\,\mathrm{ps}^{-1}\leq\Delta m_{B_s}\leq 28\,\mathrm{ps}^{-1}$. Finally we have a 1995 look at the K_L-K_S-mass difference.

PACS number(s): 12.15.Hh, 11.30.Er, 12.15.Ff, 14.65.Ha

I. INTRODUCTION

Since its discovery in the year 1964 [1] the study of CP-violation is of continuous interest to both experimentalists and theoreticians. The standard model mechanism of CP-violation involves only a single parameter, the phase δ in the Cabibbo-Kobayashi-Maskawa (CKM) matrix. Hence first the investigation of CP-violating processes is a useful tool in the determination of the CKM elements, some of which are poorly known at present. Second it may be the key to find physics beyond the standard model, once one will not be able to fit different observables with the single parameter δ.

Yet at present CP violation is only precisely and unambiguously measured in $|\Delta S|=2$ transitions. It manifests itself in the fact that the neutral kaon mass eigenstates $|K_L\rangle$ and $|K_S\rangle$ are no CP eigenstates. This indirect CP violation is characterized by the parameter

$$\varepsilon_K=\frac{\langle(\pi\pi)_{I=0}|H^{|\Delta S|=1}|K_L\rangle}{\langle(\pi\pi)_{I=0}|H^{|\Delta S|=1}|K_S\rangle}. \tag{1}$$

Its relation to the low-energy $|\Delta S|=2$ Hamiltonian $H^{|\Delta S|=2}$ is given (in the CKM phase convention for $|K^0\rangle$) by

$$\varepsilon_K=\frac{e^{i\pi/4}}{\sqrt{2}}\left(\frac{\mathrm{Im}\,\langle K^0|H^{|\Delta S|=2}|\overline{K^0}\rangle}{\Delta m_K}+\xi\right). \tag{2}$$

Here m_K is the neutral kaon mass, Δm_K is the K_L-K_S-mass difference, and ξ is a small quantity related to CP violation in the $|\Delta S|=1$ amplitudes, it contributes roughly 3% to $|\varepsilon_K|$ (see [2] for details).

The theorist's challenge is the proper inclusion of the strong interaction, which binds the quarks into hadrons and screens or enhances the CP-violating weak amplitude. Here the short distance QCD effects can be reliably calculated in renormalization-group (RG) improved perturbation theory. With our new calculation they are now completely known in the next-to-leading order (NLO). Its phenomenological implications are the subject of this paper, which is organized as follows. In the following section we present the $|\Delta S|=2$ Hamiltonian in the NLO. The further ingredients of the phenomenological analysis are discussed in Sec. III. In Sec. IV we analyze which region of the standard model parameters is compatible with the observed value for ε_K. In Sec. V we first determine the CKM phase δ from ε_K. Then we obtain $|V_{td}|$, which is a key quantity for B_d^0-$\overline{B_d^0}$ mixing, and discuss the additional constraints obtained from the measured B_d^0-$\overline{B_d^0}$ mixing parameter x_d. From $|V_{td}|$ we then predict the mass difference Δm_{B_s} of the B_s^0 system and the

*Electronic address: herrl@feynman.t30 physik, tu-muenchen.de
†Electronic address: nierste@feynman t30, physik.tu-muenchen.de

B_s^0-$\overline{B_s^0}$ mixing parameter x_s. Further we determine the improved Wolfenstein parameters $\bar{\rho}$ and $\bar{\eta}$ and further $\mathrm{Im}\,\lambda_t$, which is proportional to the Jarlskog measure of CP violation and therefore enters all CP-violating quantities in the standard model. Finally we discuss the short distance contributions to the K_L-K_S mass difference.

II. THE $|\Delta S|=2$ HAMILTONIAN IN THE NEXT-TO-LEADING ORDER

The low-energy Hamiltonian inducing K^0-$\overline{K^0}$ mixing reads

$$H^{|\Delta S|=2} = \frac{G_F^2}{16\pi^2} M_W^2 [\lambda_c^2 \eta_1 x_c + \lambda_t^2 \eta_2 S(x_t) + 2\lambda_c\lambda_t \eta_3 S(x_c, x_t)] b(\mu) Q_{S2}(\mu) + \text{H.c.} \quad (3)$$

Here G_F is the Fermi constant, M_W is the W boson mass, and $x_i = m_i^2/M_W^2$;

$$\lambda_j = V_{jd} V_{js}^* \quad (4)$$

comprises the CKM factors and Q_{S2} is the local four-quark operator

$$Q_{S2} = [\bar{s}_j \gamma_\mu (1-\gamma_5) d_j][\bar{s}_k \gamma^\mu (1-\gamma_5) d_k] = (\bar{s}d)_{V-A} (\bar{s}d)_{V-A} \quad (5)$$

with j and k being color indices. The Inami-Lim functions [3]

$$S(x_t) = x_t \left[\frac{1}{4} + \frac{9}{4}\frac{1}{1-x_t} - \frac{3}{2}\frac{1}{(1-x_t)^2}\right] - \frac{3}{2}\left[\frac{x_t}{1-x_t}\right]^3 \ln x_t,$$

$$S(x_c, x_t) = -x_c \ln x_c + x_c \left[\frac{x_t^2 - 8x_t + 4}{4(1-x_t)^2} \ln x_t + \frac{3}{4}\frac{x_t}{x_t - 1}\right] \quad (6)$$

depend on the masses of the charm and top quark and describe the $|\Delta S|=2$ transition amplitude in the absence of strong interaction.

The short distance QCD corrections are comprised in the coefficients η_1, η_2, and η_3 with a common factor $b(\mu)$ split off. They are functions of the charm- and top-quark masses and of the QCD scale parameter $\Lambda_{\overline{\mathrm{QCD}}}$. Further they depend on various renormalization scales. This dependence, however, is artificial, as it originates from the truncation of the perturbation series, and diminishes order-by-order in α_s. The η_i's have been calculated in the leading-logarithmic approximation by Gilman and Wise [4] for the case of a light top quark. The corresponding results for a heavy top quark have been derived in [5]. We briefly recall the motivation for the calculation in the NLO.

(i) To make use of the fundamental QCD scale parameter $\Lambda_{\overline{MS}}$ one must calculate beyond the leading order (LO).

(ii) The quark mass dependence of the η_i's is not accurately reproduced by the LO expressions. Especially the m_t-dependent terms in $\eta_3 S(x_c, x_t)$ belong to the NLO.

(iii) The LO results for η_1 and η_3 show a large dependence on the renormalization scales, at which one integrates out heavy particles. In the NLO these uncertainties are reduced.

(iv) One must go to the NLO to judge whether perturbation theory works, i.e., whether the radiative corrections are small. After all the corrections can be sizable. In the NLO one has to take care of the proper definition of the quark masses. It is most useful to define the η_i's with respect to running masses in the $\overline{MS}$ scheme normalized as $m_i^\star = m_i(m_i)$, i.e., we use $x_i^\star = [m_i(m_i)]^2/M_W^2$ in (3) and mark the corresponding η_i's with a star. The NLO calculation here requires the use of the one-loop relation between the pole mass and the running mass:

$$m^{\mathrm{pole}} = m^\star \left(1 + \frac{\alpha_s(m^\star)}{\pi}\frac{4}{3}\right).$$

The top-quark running mass $m_t^\star$ is smaller than m_t^{pole} by 8 GeV.

$\eta_2^\star$ and $\eta_3^\star$ depend very weakly on the charm- and top-quark mass and on $\Lambda_{\overline{MS}}^{\mathrm{NLO}}$, so that they can be treated as constants. In contrast $\eta_1^\star$ is a steep function of $m_c^\star$ and $\Lambda_{\overline{MS}}^{\mathrm{NLO}}$.

Now the NLO values read

$$\eta_1^\star = 1.32^{+0.21}_{-0.23}, \quad \eta_2^\star = 0.57^{+0.00}_{-0.01}, \quad \eta_3^\star = 0.47^{+0.03}_{-0.04} \quad (7)$$

where $m_c^\star = 1.3\,\mathrm{GeV}$ and $\Lambda_{\overline{MS}}^{\mathrm{NLO}} = 0.310\,\mathrm{GeV}$ have been used. The quoted theoretical errors are estimated in two ways: First the renormalization scales have been varied and second the calculated $O(\alpha_s)$ corrections have been squared.

The calculation for $\eta_1^\star$ has been performed by us [6] and $\eta_2^\star$ has been obtained by Buras, Jamin, and Weisz [7]. The NLO value for $\eta_3^\star$ in (7) is new. We will present details of the calculation in [8].

For comparison we give the old leading-order central values [4]

$$\eta_1^{\star\,\mathrm{LO}} = 0.80, \quad \eta_2^{\star\,\mathrm{LO}} = 0.62, \quad \eta_3^{\star\,\mathrm{LO}} = 0.36. \quad (8)$$

The common factor of the short distance QCD corrections split off in (3) equals

$$b(\mu) = [\alpha_s(\mu)]^{-2/9} \left(1 + \frac{307}{162}\frac{\alpha_s(\mu)}{4\pi}\right) \quad (9)$$

in the NLO. Here μ is the scale at which the perturbative short distance calculation is matched to the nonperturbative evaluation of the hadronic matrix element. The

latter must compensate the μ dependence in (9) and is parametrized by B_K as

$$\langle \overline{K^0}|Q_{S2}(\mu)|K^0\rangle = \frac{8}{3} f_K^2 m_K^2 B_K / b(\mu). \tag{10}$$

Here m_K and f_K are the mass and decay constant of the neutral kaon.

III. MISCELLANEOUS

A. CKM matrix and unitarity triangle

For all numerical analyses we will use the exact standard parametrization of the CKM matrix [9]:

$$V = \begin{pmatrix} V_{ud} & V_{us} & V_{ub} \\ V_{cd} & V_{cs} & V_{cb} \\ V_{td} & V_{ts} & V_{tb} \end{pmatrix} = \begin{pmatrix} c_{12}c_{13} & s_{12}c_{13} & s_{13}e^{-i\delta} \\ -s_{12}c_{23} - c_{12}s_{23}s_{13}e^{i\delta} & c_{12}c_{23} - s_{12}s_{23}s_{13}e^{i\delta} & s_{23}c_{13} \\ s_{12}s_{23} - c_{12}c_{23}s_{13}e^{i\delta} & -c_{12}s_{23} - s_{12}c_{23}s_{13}e^{i\delta} & c_{23}c_{13} \end{pmatrix}, \tag{11}$$

where $c_{ij} = \cos\theta_{ij}$ and $s_{ij} = \sin\theta_{ij}$.

The unitarity of V provides us with many relations among its elements. The most useful one is

$$V_{ud}V_{ub}^* + V_{cd}V_{cb}^* + V_{td}V_{tb}^* = 0. \tag{12}$$

With

$$\bar{\rho} = -\mathrm{Re}\,\frac{V_{ud}V_{ub}^*}{V_{cd}V_{cb}^*}, \qquad \bar{\eta} = -\mathrm{Im}\,\frac{V_{ud}V_{ub}^*}{V_{cd}V_{cb}^*} \tag{13}$$

(12) describes a *unitarity triangle* in the complex $\bar{\rho}$-$\bar{\eta}$ plane, whose edges are located at the points $(0,0)$, $(0,1)$, and $(\bar{\rho},\bar{\eta})$ (see Fig. 1).

To illustrate the size of the contributions from the different CKM elements we will also use the improved Wolfenstein parametrization [10], which is obtained from (11) by defining the parameters λ, A, ρ, and η by

$$s_{12} = \lambda = 0.22, \qquad s_{23} = A\lambda^2,$$
$$s_{13}e^{-i\delta} = A\lambda^3(\rho - i\eta),$$

and expanding the cosines in (11) to any desired order in $\lambda = 0.22$. The expansion to order λ^3 yields the conventional Wolfenstein parametrization [11]. Yet it is well known that the proper treatment of CP-violating effects requires a higher accuracy:

$$V = \begin{pmatrix} 1 - \frac{\lambda^2}{2} & \lambda & A\lambda^3(\rho - i\eta) \\ -\lambda - iA^2\lambda^5\eta & 1 - \frac{\lambda^2}{2} & A\lambda^2 \\ A\lambda^3(1 - \bar{\rho} - i\bar{\eta}) & -A\lambda^2 - iA\lambda^4\eta & 1 \end{pmatrix} \tag{14}$$

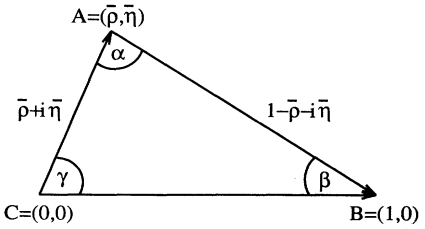

FIG. 1. The unitarity triangle of (13).

is exact to order λ^3 and contains the phenomenologically important terms up to the order λ^5 [10]. Here $\bar{\rho}$ and $\bar{\eta}$ defined in (13) are expanded as

$$\bar{\rho} = \rho\left(1 - \frac{\lambda^2}{2} + O(\lambda^4)\right), \quad \bar{\eta} = \eta\left(1 - \frac{\lambda^2}{2} + O(\lambda^4)\right).$$

B. CKM elements from ε_K

The experimental value for $|\varepsilon_K|$ [9],

$$|\varepsilon_K| = (2.266 \pm 0.023) \times 10^{-3}, \tag{15}$$

constrains the CKM elements with (2), (3), and (10) via

$$1.21 \times 10^{-7} = B_K[-\mathrm{Im}\,\lambda_c^2\,\eta_1^\star\,S(x_c^\star) - \mathrm{Im}\,\lambda_t^2\,\eta_2^\star\,S(x_t^\star) - 2\,\mathrm{Im}\,(\lambda_c\lambda_t)\,\eta_3^\star\,S(x_c^\star, x_t^\star)]. \tag{16}$$

Here the number on the left-hand side (lhs) originates from

$$1.21 \times 10^{-7} = \frac{12\sqrt{2}\,\pi^2\,\Delta m_K}{G_F^2\,F_K^2\,m_K\,M_W^2}\left(|\varepsilon_K| - \frac{\xi}{\sqrt{2}}\right)$$

with the numerical values for these physical quantities listed in Sec. III C. Further λ_j has been defined in (4) and the small term ξ in (2) has been estimated with the help of [12] to contribute roughly -3% to ε_K. The uncertainty in the lhs due to experimental errors is about 1% and therefore negligible compared to the uncertainties to be discussed in Sec. III C.

The relative importance of the three terms in the square brackets in (16) can be demonstrated with the help of the improved Wolfenstein parametrization (14) turning (16) into

$$5.3 \times 10^{-4} = B_K A^2 \bar{\eta}[(1 - \bar{\rho})A^2\lambda^4\eta_2^\star S(x_t^\star) + \eta_3^\star S(x_c^\star, x_t^\star) - \eta_1^\star x_c^\star] \tag{17}$$

after dividing both sides by $2\,\lambda^6$. In (17) one sees that the top-top contribution is CKM suppressed by four powers

of λ, but this suppression is overcompensated because the top quark is so heavy:

$$\eta_2^\star S(x_t^\star) \approx 1.3 \times 10^3 \eta_3^\star S(x_c^\star, x_t^\star) \approx 4 \times 10^3 \eta_1^\star x_c^\star.$$

Hence $\eta_2^\star$ is the most important short distance coefficient, $\eta_3^\star$ is second relevant, and $\eta_1^\star$ contributes least. Their contributions to the right-hand side (rhs) of (17) are roughly 75%, 37%, and -12%. Yet if we look at the changes in the $\eta_i^\star$'s due to the NLO calculations [cf. (7) and (8)] one realizes that the NLO correction to $\eta_3^\star$ is the most important one, because it is enhanced by 30%, while $\eta_2^\star$ has decreased by only 8%.

C. Ranges for the input parameters

In this section we will discuss the actual ranges of the input parameters needed for our analysis. To determine δ from (16) one must first fix the three angles in (11) from the magnitudes of three CKM elements. While $|V_{us}| = 0.2205 \pm 0.0018$ is well known [9], the determination of V_{cb} and especially V_{ub} from tree-level b decays is still plagued by sizable experimental and theoretical uncertainties. Since these parameters are two main contributors to our final error bars, we will now consider them in more detail

The theoretical understanding of the determination of V_{cb} from exclusive and inclusive B decays has recently made significant progress [13]. In [13] presumably large perturbative corrections proportional to $\alpha_s^{n+1}\beta_0^n$ have been summed to all orders in the decay rate resolving both the previous discrepancy between the results of inclusive and exclusive analyses and the large scheme dependence of the inclusive analysis found in [15]. With $\tau_{B_d^0} = (1.59 \pm 0.07)$ ps [16] the result of [13] reads

$$V_{cb} = 0.040 \pm 0.003 \tag{18}$$

coinciding with the result presented in [14]. $b \to u$ decays are harder to treat both theoretically and experimentally. We will use [9]

$$\left|\frac{V_{ub}}{V_{cb}}\right| = 0.08 \pm 0.02. \tag{19}$$

A further ingredient of our analysis is the top-quark mass, which has been determined in the CDF experiment [17] to equal

$$m_t^{\text{pole}} = (176 \pm 13)\,\text{GeV}.$$

In NLO analyses one has to take into account the proper definition of the mass: The corresponding value for the running mass in the $\overline{MS}$ scheme is

$$m_t^\star = m_t(m_t) = (168 \pm 13)\,\text{GeV}. \tag{20}$$

The fit of the top mass from the LEP data yields the same central value with an error bar of roughly the double size [18]. The D0 group finds $m_t^{\text{pole}} = (199 \pm 30)$ GeV [19]. Yet the analysis in [20] extracting the top mass by partly fitting the cross sections finds a lower value $m_t^{\text{pole}} = (170 \pm 9)$ GeV from the combined analysis of CDF and D0. Therefore the range given in (20) well represents the possible values for $m_t^\star$ and will be used in the following sections.

Next we have to discuss the nonperturbative parameter B_K defined in (10): The size of B_K has been the subject of a controversial discussion during the last decade. The $1/N_c$ result $B_K = 0.7 \pm 0.1$ [21] was in contradiction with lower values estimated with chiral symmetry [22] or the QCD hadron duality approach [23]. Yet a recent analysis [24] has vindicated the result of [21] and seems to have explained the difference to the estimates in [22,23]. Further recent quenched QCD lattice calculations have yielded values around $B_K = 0.78$ (see [25] and references therein). The effect of dynamical fermions has been found to be small in [26]. We will therefore use the following range in our calculation:

$$B_K = 0.75 \pm 0.10. \tag{21}$$

In fact we will see in Sec. IV that the inclusion of values lower than $B_K = 0.65$ can only very hardly be brought into agreement with the measured value of ε_K. We remark that the NLO short distance calculation also affects B_K because of the factor of $1/b(\mu)$ on the rhs of (10). Nonperturbative calculations determine the matrix element on the lhs of (10) and usually the quoted results for B_K are obtained with the leading order factor $b^{\text{LO}}(\mu) = \left[\alpha^{\text{LO}}(\mu)\right]^{-2/9}$ instead of the NLO value given in (9). Hence in a consistent NLO analysis one should correct for this by multiplying the cited values with $b(\mu)/b^{\text{LO}}(\mu)$. Yet numerically this amounts to a change of about 3% for $\mu = O\,(0.7\,\text{GeV})$ and can be neglected in view of the larger uncertainty in (21). But once the lattice results will achieve an accuracy in the percentage region they should be quoted with the NLO factor given in (9).

At this point it is instructive to investigate the impact of our NLO calculation for $\eta_3^\star$: With (16) one can easily verify that the shift from $\eta_3^{\star\,\text{LO}} = 0.36$ in (8) to $\eta_3^\star = 0.47$ in (7) has the same influence on $|\varepsilon_K|$ as a shift from $B_K = 0.82$ to $B_K = 0.75$. In the same way one can estimate the uncertainty caused by the error bar in the NLO values in (7): The remaining uncertainties in the NLO $\eta_i^\star$'s correspond to a change in B_K by ± 0.02.

Let us now look at the other input parameters. The dominant QCD factors $\eta_2^\star$ and $\eta_3^\star$ depend very weakly on the QCD scale parameter $\Lambda_{\overline{MS}}^{\text{NLO}}$, which therefore hardly affects our results for ε_K. Yet of course the determination of the input parameters V_{cb} and $|V_{ub}/V_{cb}|$ depends on $\Lambda_{\overline{MS}}^{\text{NLO}}$; this uncertainty is included in the error bar in (18) and (19) [13]. Conversely the K_L-K_S mass difference discussed in Sec. VI is dominated by $\eta_1^\star$ which is a steep function of $\Lambda_{\overline{MS}}^{\text{NLO}}$. We will consider [27]

$$\Lambda_{\overline{MS}}^{\text{NLO}} = (310 \pm 100)\,\text{MeV} \tag{22}$$

corresponding to

$$\alpha(M_Z) = 0.117 \pm 0.006. \quad (23)$$

The situation is the same with respect to the dependence on $m_c^\star$: The rhs of (16) depends only weakly on $m_c^\star$. Varying [13]

$$m_c^\star = (1.29 \pm 0.07)\,\text{GeV} \quad (24)$$

within the quoted range affects the rhs of (16) by 3%, i.e., it is negligible compared to the uncertainty in B_K. Yet the K_L-K_S mass difference depends on $m_c^\star$ sizably.

For completeness we list the remaining parameters entering the analysis of ε_K [9]:

$$G_F = 1.17 \times 10^{-5}\,\text{GeV}^{-2}, \quad F_K = 161\,\text{MeV},$$
$$m_K = 498\,\text{MeV}, \quad \Delta m_K = 3.52 \times 10^{-15}\,\text{GeV},$$
$$M_W = 80.22\,\text{GeV}, \quad m_b^\star = 4.2\,\text{GeV}$$

and the measured value for $|\varepsilon_K|$ has been given in (15). The uncertainties of these quantities are irrelevant for the analysis.

Finally we list the additional input parameters needed for the B^0-$\overline{B^0}$ mixing: The $B_d^0\overline{B_d^0}$ mixing parameter $x_d = 0.78 \pm 0.05$ enters the calculation in the combination

$$\Delta m_{B_d} = x_d/\tau_{B_d} = (0.496 \pm 0.032)\ \text{ps}^{-1}, \quad (25)$$

which is the world average presented in [16]. Yet the largest uncertainty is due to the hadronic parameters F_{B_d} and B_{B_d} appearing in the form

$$F_{B_d}\sqrt{B_{B_d}} = (195 \pm 45)\,\text{MeV}. \quad (26)$$

This result has been obtained with lattice methods [28] and QCD sum rules [29]. The ratio F_{B_s}/F_{B_d} has been well determined from the lattice [28]

$$\frac{F_{B_s}}{F_{B_d}} = 1.22 \pm 0.04. \quad (27)$$

Further we will need the meson masses $m_{B_d} = 5.28\,\text{GeV}$ and $m_{B_s} = 5.38\,\text{GeV}$ and the B_s lifetime $\tau_{B_s} = (1.53 \pm 0.10)$ ps [16].

IV. BOUNDS ON STANDARD MODEL PARAMETERS

As explained in the previous section the final error bar of the CKM phase δ determined from ε_K is due to the uncertainties in V_{cb}, $|V_{ub}/V_{cb}|$, B_K, and $m_t^\star$. Yet it is well known that the unitarity of the CKM matrix constrains the allowed range for these four quantities: If one fixes three of them, a lower bound for the fourth one can be obtained, because otherwise (16) yields no real solutions for $\cos\delta$. In terms of the improved Wolfenstein parameters (14) these solutions appear as the intersection points of a hyperbola with a circle. The lower bound solution corresponds to a set of parameters for which the hyperbola touches the circle in one point (see [10] for details). Prior to the discovery of the top quark this method was used to find a lower bound on the top-quark mass (see, e.g., [10,30]). Now in the top era it is more useful to determine the allowed region for the other two fundamental standard model parameters in the game, V_{cb} and $|V_{ub}/V_{cb}|$. This is shown in Fig. 2. The ranges (18) and (19) correspond to a rectangle in Fig. 2. For each pair $(m_t^\star, B_K)$ the constraint from ε_K defines a curve in Fig. 2 such that only the region above this curve is allowed.

We emphasize that the central values for the input parameters given in (18) to (21) are close to the borderline curve depicted in Fig. 2. With the old LO value for η_3 the central values would even seem to contradict the measured value for ε_K. The minimal value for $|V_{ub}/V_{cb}|$ equals 0.0778, if the central values in (18), (20), and (21) are chosen for the other parameters. Conversely the minimal values for the other parameters read $V_{cb,\,\text{min}} = 0.397$, $m_{t,\,\text{min}}^\star = 164\,\text{GeV}$, and $B_{K,\,\text{min}} = 0.729$, if the remaining three ones equal the central values chosen in Sec. III C. Of course varying these parameters to higher values relaxes the lower bound on the fourth one. Altogether the constraint from ε_K rules out almost one half of the parameter space of Sec. III C.

From these remarks it is clear that ε_K strongly constrains those extensions of the standard model, in which extra CP-violating interactions *diminish* $|\varepsilon_K|$, because then the standard model contribution $|\varepsilon_K^{\text{SM}}|$ must be larger to accommodate for the measured value of $|\varepsilon_K|$. The lower bound can be summarized in the following approximate formula:

$$\frac{V_{cb}}{0.0397}\left(\frac{|V_{ub}/V_{cb}|}{0.080}\right)^{0.27}\left(\frac{m_t^\star}{168\,\text{GeV}}\right)^{0.31}\left(\frac{B_K}{0.75}\right)^{0.27} \times \left(\frac{2.27 \times 10^{-3}}{|\varepsilon_K^{\text{SM}}|}\right)^{0.27} \geq 1. \quad (28)$$

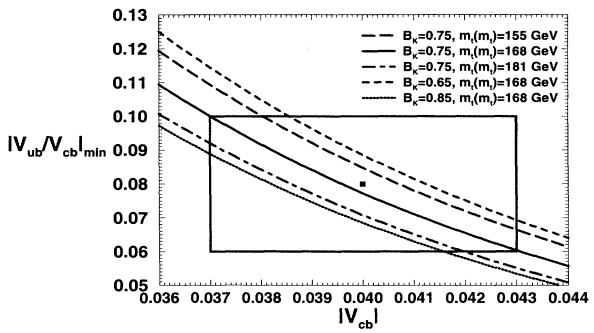

FIG. 2. New physics borderlines for various values of $m_t^\star$ and B_K. Each pair $(m_t^\star, B_K)$ defines a curve. If the standard model is the only source of indirect CP violation in the neutral kaon system, the points below the curve are excluded. The solid line in the middle corresponds to the central values for $m_t^\star$ and B_K given in Sec. III C. The rectangle limits the allowed range for V_{cb} and $|V_{ub}/V_{cb}|$ obtained from tree-level b decays according to (18) and (19). The point in the middle of the rectangle corresponds to the central values in (18) and (19).

$|V_{ub}/V_{cb}|_{\min}$ determined from (28) concides with the exact solution to 4% accuracy in the parameter range of Sec. III C. For $0.039 \leq V_{cb} \leq 0.041$ the agreement is better than 2%.

(28) displays the sensitivity of our analysis on V_{cb}. Although V_{cb} is known to a much higher accuracy than $|V_{ub}/V_{cb}|$, its uncertainty contributes roughly as much to the final error as the one of $|V_{ub}/V_{cb}|$. The situation is similar in the analysis of Sec. V.

Finally we remark that in the vicinity of the lower bound values the determination of the CKM elements is very sensitive to the input parameters. Because of the required precision one should use the exact parametrization (11) of the CKM matrix here.

V. CKM MATRIX PHENOMENOLOGY

In this section we determine various CKM parameters using $|\varepsilon_K|$ and the unitarity of the CKM matrix and discuss the constraints following from B^0-$\overline{B^0}$ mixing.

A. The CKM phase δ

By solving Eq. (16) for $\cos\delta$ we calculate the two solutions for the phase δ of the CKM matrix. For the input parameters defined in Sec. III C the resulting δ's have been compiled into Table I, where the dependence on the key parameters $m_t^\star$, B_K, V_{cb}, and $|V_{ub}/V_{cb}|$ is made explicit. A dash means that there exists no solution for these parameters, lines which do not contain a solution at all have been omitted from the table. This happens for small values of the above-mentioned input parameters and served to derive the bounds on these parameters in Sec. IV.

For our central values we observe the two solutions being very close to the limits derived in Sec. IV. This leads to very asymmetric error bars. Therefore we first give the central values and the variation of it for all relevant parameters separately:

$$\begin{aligned}\delta^{\rm low} &= 89^\circ \begin{matrix}+13^\circ & +13^\circ & +13^\circ & +13^\circ\\ -28^\circ & -23^\circ & -14^\circ & -17^\circ\end{matrix},\\ \delta^{\rm high} &= 116^\circ \begin{matrix}+24^\circ & +24^\circ & +12^\circ & +15^\circ\\ -13^\circ & -13^\circ & -13^\circ & -13^\circ\end{matrix}.\end{aligned} \tag{29}$$

The variations in (29) are meant as follows: The first number in the lower line for $\delta^{\rm low}$ and the first number in the upper line for $\delta^{\rm high}$ are the two solutions obtained by pushing V_{cb} to its maximal value $V_{cb} = 0.043$ while keeping the other three parameters fixed to their central values given in Sec. III C. Conversely the other three numbers in these lines represent the variation when the same is done for $|V_{ub}/V_{cb}|$, $m_t^\star$, and B_K. In contrast moving the key parameters to lower values makes the two solutions for δ approach until they merge, when the varied parameter reaches its "lower bound value" discussed in the preceding section. The variations on the upper line for $\delta^{\rm low}$ and the lower line for $\delta^{\rm high}$ correspond to these values, which are $V_{cb,\min} = 0.0397$, $|V_{ub}/V_{cb}|_{\min} = 0.0778$, $m^\star_{t,\min} = 164\,\text{GeV}$, and $B_{K,\min} = 0.729$.

We combine the individual variations in (29) to

$$\begin{aligned}\delta^{\rm low} &= 89^{\circ\,+13^\circ}_{\quad -43^\circ},\\ \delta^{\rm high} &= 116^{\circ\,+39^\circ}_{\quad -13^\circ}.\end{aligned} \tag{30}$$

The error in the lines stemming from the lower bounds is motivated by the observation that the value $\delta = 103^\circ$ for which the two solutions merge is essentially independent of the input parameters. The error in the lines emerging from pushing the input parameters to their maximally allowed values is obtained by adding the four individual variations of (29) in quadrature. This seems questionable, because the theoretical errors of the input parameters may be correlated. Hence we have also determined the error by finding simply the maximal value for $\delta^{\rm high}$ and the minimal value for $\delta^{\rm low}$ when all input quantities are varied within the ranges given in Sec. III C. These extremal values correspond to the point ($V_{cb} = 0.043, |V_{ub}/V_{cb}| = 0.10, m_t^\star = 181\,\text{GeV}, B_K = 0.85$), because $\delta^{\rm high}$ and $\delta^{\rm low}$ are monotonous functions of all four arguments. This results in an error which is only slightly larger than the one cited in (30), -48° instead of -43° in $\delta^{\rm low}$ and $+42^\circ$ instead of $+39^\circ$ in $\delta^{\rm high}$. This is caused by the fact that δ varies only very slowly in the parameter region far away from the central values. $|V_{td}|$ discussed in the following section shows the same behavior, which is evident from the plots in Fig. 3 and Fig. 4. Hence the error bars in (30) are clearly not too small.

Let us now remark that in Table I the error resulting from the variation of the other parameters entering the calculation is not shown. It amounts to roughly 3–4°.

The discussion of δ is especially instructive in conjunction with the unitarity triangle. We will therefore return to δ in Sec. V E, where we will also see that the ad-

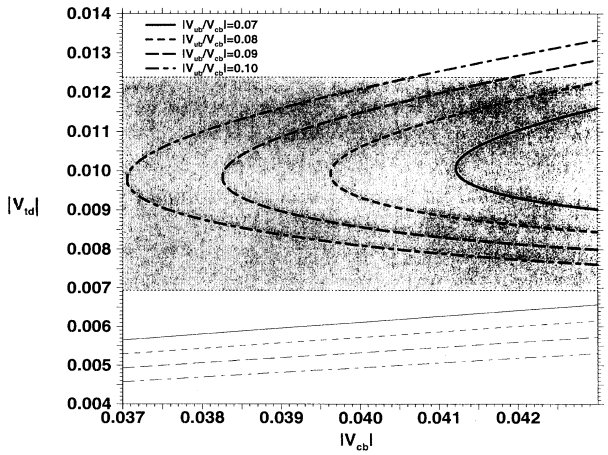

FIG. 3. The dependence of $|V_{td}|$ on V_{cb} for $B_K = 0.75$, $m_t^\star = 168\,\text{GeV}$, and four values of $|V_{ub}/V_{cb}|$. The thin lines correspond to $\delta = 0$, i.e., no CP violation. The shaded area is consistent with x_d from (34).

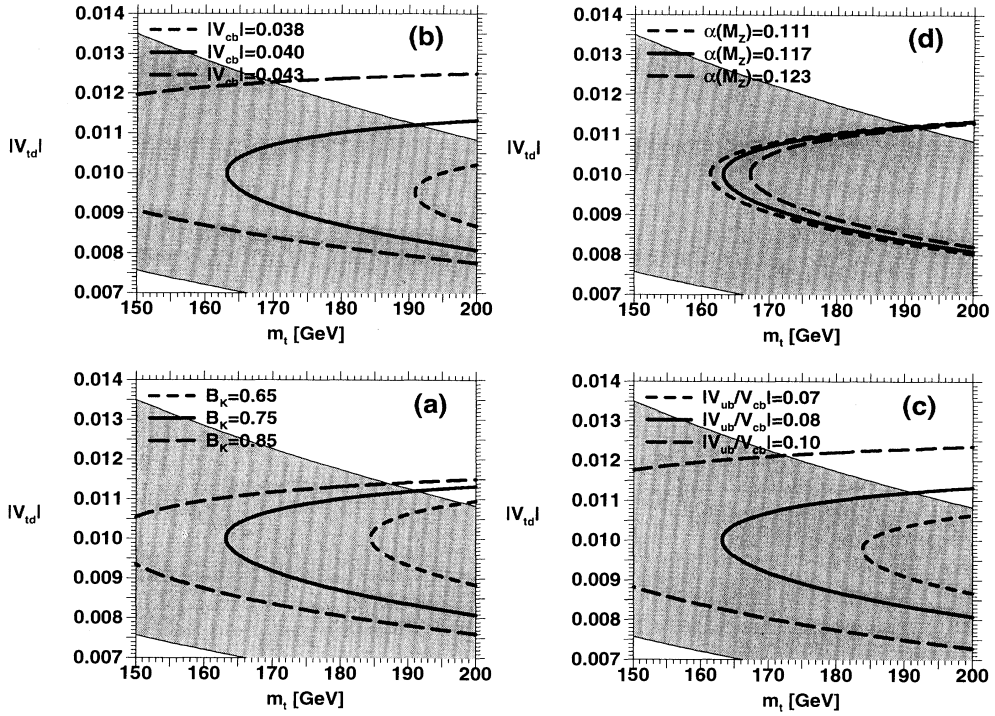

FIG. 4. The dependence of $|V_{td}|$ on $m_t^\star$ for three values of (a) B_K, (b) V_{cb}, (c) $|V_{ub}/V_{cb}|$, and (d) $\alpha(M_Z)$. All other parameters equal their central values of Sec. III C. The shaded area gives the band (34) of $|V_{td}|$'s allowed by the B_d^0-$\overline{B_d^0}$ mixing parameter x_d. For large values of the discussed parameters x_d favors the smaller branch of the solution.

TABLE I. The two solutions for the phase δ of the CKM matrix in degrees as a function of $m_t^\star$, B_K, $|V_{ub}/V_{cb}|$, and $|V_{cb}|$. A dash means no solution. Lines with no solutions at all have been omitted. Values for other input parameters may be calculated by linear interpolation.

		V_{cb}	0.037	0.038	0.039	0.040	0.041	0.042	0.043
$m_t^\star$	B_K	$\left\|\frac{V_{ub}}{V_{cb}}\right\|$				δ			
155	0.65	0.08	—	—	—	—	—	—	86 120
155	0.65	0.09	—	—	—	—	98 110	81 126	72 133
155	0.65	0.10	—	—	—	92 118	79 129	71 136	65 141
155	0.75	0.07	—	—	—	—	—	—	83 119
155	0.75	0.08	—	—	—	—	90 115	77 127	69 134
155	0.75	0.09	—	—	—	85 122	75 131	67 137	61 142
155	0.75	0.10	—	—	83 126	74 134	67 140	61 144	56 148
155	0.85	0.06	—	—	—	—	—	—	89 111
155	0.85	0.07	—	—	—	—	93 110	77 124	68 132
155	0.85	0.08	—	—	—	83 121	73 130	65 137	59 141
155	0.85	0.09	—	96 111	80 126	71 134	64 140	58 144	53 148
155	0.85	0.10	92 117	79 129	70 136	64 142	58 146	53 149	49 152
168	0.65	0.07	—	—	—	—	—	—	95 109
168	0.65	0.08	—	—	—	—	—	84 121	74 130
168	0.65	0.09	—	—	—	96 113	80 127	72 134	65 140
168	0.65	0.10	—	—	91 119	79 130	71 137	65 142	59 146
168	0.75	0.07	—	—	—	—	—	82 121	72 130
168	0.75	0.08	—	—	—	89 116	76 128	68 135	62 140
168	0.75	0.09	—	—	85 123	74 132	67 138	61 143	56 147
168	0.75	0.10	—	83 126	73 134	66 140	61 144	56 148	51 151
168	0.85	0.06	—	—	—	—	—	86 114	74 126
168	0.85	0.07	—	—	—	91 112	76 125	68 133	61 138
168	0.85	0.08	—	—	83 122	72 131	65 137	59 142	54 146
168	0.85	0.09	97 111	80 127	71 134	64 140	58 144	53 148	49 151
168	0.85	0.10	79 129	70 136	64 142	58 146	53 150	49 153	45 155
181	0.65	0.07	—	—	—	—	—	94 111	78 125
181	0.65	0.08	—	—	—	—	84 122	74 131	66 137
181	0.65	0.09	—	—	97 112	81 127	72 135	65 140	59 144
181	0.65	0.10	—	93 118	80 130	71 137	65 142	59 146	54 150
181	0.75	0.06	—	—	—	—	—	—	78 122
181	0.75	0.07	—	—	—	—	82 121	71 130	64 136
181	0.75	0.08	—	—	90 116	77 128	68 135	62 140	56 145
181	0.75	0.09	—	86 122	75 132	67 138	61 143	55 147	51 150
181	0.75	0.10	84 125	74 134	67 140	61 145	56 148	51 151	47 154
181	0.85	0.06	—	—	—	—	86 115	73 126	65 133
181	0.85	0.07	—	—	92 111	77 126	68 133	61 139	55 143
181	0.85	0.08	—	84 121	73 131	65 137	59 142	54 146	49 150
181	0.85	0.09	81 126	71 134	64 140	58 145	53 148	49 151	45 154
181	0.85	0.10	71 136	64 142	58 146	53 150	49 153	45 155	42 158

ditional incorporation of B_d^0-$\overline{B_d^0}$ mixing yields a tighter upper bound on δ than the one in (30).

Once we have in this way obtained the phase δ from the three angles s_{12}, s_{23}, and s_{13} or equivalently V_{us}, V_{cb}, and $|V_{ub}/V_{cb}|$, we are by use of (11) able to derive combinations of CKM elements, which are of special phenomenological interest.

B. $|V_{td}|$

$|V_{td}|$ plays an important role for the parameter x_d of B_d^0-$\overline{B_d^0}$ mixing. Especially once the B_s^0-$\overline{B_s^0}$ mixing mixing parameter x_s is measured a theoretically clean determination of $|V_{td}|$ from the ratio x_s/x_d will be possible. The comparison of the result with the determination of $|V_{td}|$ from ε_K presented in the following will be a viable experimental test of the quark mixing sector.

Table II shows the value of $|V_{td}|$ as derived from δ in Table I. As usual we give both solutions, the smaller one always corresponds to the smaller value of δ and vice versa. As in the case of δ a dash means that there exists no solution for the specific set of parameters. We find for the central values and the individual variations

$$|V_{td}|^{\text{low}} \times 10^3 = 9.3\ {}^{+0.6\ +0.6\ +0.6\ +0.6}_{-0.9\ -1.3\ -0.7\ -0.9}\ ,$$
$$|V_{td}|^{\text{high}} \times 10^3 = 10.6\ {}^{+1.7\ +1.5\ +0.5\ +0.6}_{-0.6\ -0.6\ -0.5\ -0.5}\ . \quad (31)$$

The upper line of $|V_{td}|^{\text{low}}$ and the lower line of $|V_{td}|^{\text{high}}$ corresponds to $V_{cb,\min}$, $|V_{ub}/V_{cb}|_{\min}$, $m^*_{t,\min}$, and $B_{K,\min}$ [see the values in the paragraph below (29)], the lower line of $|V_{td}|^{\text{low}}$ and the upper line of $|V_{td}|^{\text{high}}$ result from putting the input parameters to their highest allowed value.

In the same way as in the case of δ in the last section, we obtained as combined errors

$$|V_{td}|^{\text{low}} \times 10^3 = 9.3^{+0.6}_{-1.9}\ ,$$
$$|V_{td}|^{\text{high}} \times 10^3 = 10.6^{+2.4}_{-0.6}\ . \quad (32)$$

Again the scanning for the extremal values yields an error which is not much larger than the addition in quadrature: -2.4 instead of -1.9 and $+2.9$ instead of $+2.4$ in (32). The extremal values again correspond to the largest values for all input parameters. We remark here that we have also used a third way to estimate the error of $|V_{td}|$: We have scanned the extremal values for $|V_{td}|$ for those parameters which lie in a 1σ ellipsoid (38) around the

TABLE II. The values of $|V_{td}|$ corresponding to the two values of δ in Table I.

m_t^*	B_K	$\left\lvert\frac{V_{ub}}{V_{cb}}\right\rvert$	V_{cb} 0.037	0.038	0.039	0.040	0.041	0.042	0.043
						$\lvert V_{td}\rvert \times^3$			
155	0.65	0.08	—	—	—	—	—	—	9.8 11.5
155	0.65	0.09	—	—	—	—	10.2 10.9	9.5 11.8	9.1 12.4
155	0.65	0.10	—	—	—	9.8 11.2	9.2 12.0	8.9 12.6	8.6 13.0
155	0.75	0.07	—	—	—	—	—	—	9.6 11.2
155	0.75	0.08	—	—	—	—	9.6 10.8	9.1 11.5	8.9 12.1
155	0.75	0.09	—	—	—	9.2 11.1	8.8 11.7	8.6 12.2	8.4 12.7
155	0.75	0.10	—	—	9.0 11.3	8.6 11.9	8.3 12.4	8.1 12.8	8.0 13.2
155	0.85	0.06	—	—	—	—	—	—	9.8 10.7
155	0.85	0.07	—	—	—	—	9.6 10.4	9.1 11.2	8.9 11.7
155	0.85	0.08	—	—	—	9.0 10.8	8.7 11.4	8.5 11.9	8.3 12.3
155	0.85	0.09	—	9.4 10.1	8.7 11.0	8.4 11.6	8.1 12.0	8.0 12.5	7.9 12.8
155	0.85	0.10	9.0 10.3	8.5 11.1	8.2 11.7	7.9 12.1	7.7 12.6	7.6 13.0	7.5 13.4
168	0.65	0.07	—	—	—	—	—	—	10.2 10.8
168	0.65	0.08	—	—	—	—	—	9.5 11.3	9.2 12.0
168	0.65	0.09	—	—	—	9.8 10.7	9.2 11.6	8.8 12.1	8.6 12.6
168	0.65	0.10	—	—	9.5 11.0	9.0 11.7	8.6 12.3	8.4 12.8	8.2 13.2
168	0.75	0.07	—	—	—	—	—	9.3 11.0	9.0 11.6
168	0.75	0.08	—	—	—	9.3 10.6	8.9 11.3	8.6 11.8	8.5 12.3
168	0.75	0.09	—	—	9.0 10.9	8.6 11.5	8.3 12.0	8.1 12.4	8.0 12.8
168	0.75	0.10	—	8.8 11.0	8.4 11.6	8.1 12.1	7.9 12.5	7.7 12.9	7.6 13.3
168	0.85	0.06	—	—	—	—	—	9.4 10.5	9.1 11.2
168	0.85	0.07	—	—	—	9.3 10.2	8.8 10.9	8.6 11.4	8.5 11.9
168	0.85	0.08	—	—	8.8 10.6	8.4 11.1	8.2 11.6	8.1 12.0	8.0 12.4
168	0.85	0.09	9.2 9.8	8.5 10.7	8.1 11.3	7.9 11.7	7.8 12.2	7.7 12.6	7.6 12.9
168	0.85	0.10	8.3 10.8	8.0 11.4	7.7 11.8	7.5 12.3	7.4 12.7	7.3 13.1	7.2 13.4
181	0.65	0.07	—	—	—	—	—	9.9 10.6	9.3 11.4
181	0.65	0.08	—	—	—	—	9.3 11.1	8.9 11.7	8.7 12.2
181	0.65	0.09	—	—	9.6 10.4	9.0 11.3	8.6 11.9	8.4 12.3	8.2 12.8
181	0.65	0.10	—	9.3 10.7	8.8 11.4	8.4 12.0	8.2 12.5	8.0 12.9	7.8 13.3
181	0.75	0.06	—	—	—	—	—	—	9.3 11.0
181	0.75	0.07	—	—	—	—	9.1 10.8	8.8 11.3	8.6 11.8
181	0.75	0.08	—	—	9.1 10.3	8.7 11.0	8.4 11.5	8.2 12.0	8.1 12.4
181	0.75	0.09	—	8.8 10.6	8.4 11.2	8.1 11.7	7.9 12.1	7.8 12.5	7.7 12.9
181	0.75	0.10	8.6 10.7	8.2 11.3	7.9 11.8	7.7 12.2	7.6 12.6	7.4 13.0	7.3 13.4
181	0.85	0.06	—	—	—	—	9.2 10.3	8.9 10.9	8.7 11.4
181	0.85	0.07	—	—	9.1 9.9	8.6 10.7	8.4 11.2	8.3 11.6	8.2 12.0
181	0.85	0.08	—	8.6 10.3	8.2 10.9	8.0 11.3	7.9 11.8	7.8 12.1	7.7 12.5
181	0.85	0.09	8.3 10.4	8.0 11.0	7.8 11.5	7.6 11.9	7.5 12.3	7.4 12.6	7.3 13.0
181	0.85	0.10	7.8 11.1	7.6 11.5	7.4 12.0	7.2 12.4	7.1 12.7	7.0 13.1	7.0 13.5

central values. This has yielded the same error bar as in (32). Yet for the determination of the quantities to be discussed in the following sections this method is most useful.

Let us discuss the dependence of $|V_{td}|$ on the most important input parameters in more detail. In Fig. 3 we plot the dependence of $|V_{td}|$ on V_{cb} for $|V_{ub}/V_{cb}| = 0.07, 0.08, 0.09, 0.10$ and the other parameters being fixed at their central values. For $|V_{ub}/V_{cb}| = 0.06$ we cannot find a solution. The curves drawn with thick lines represent the actual solution for $|V_{td}|$, the thin lines display the value of $|V_{td}|$, if the phase δ would be equal to zero.

Let us further compare this to the bound on $|V_{td}|$ which we get from B_d^0-$\overline{B_d^0}$ mixing. The experimentally measured quantities Δm_{B_d} and x_d are given by

$$\Delta m_{B_d} = x_d/\tau_{B_d} = |V_{td}|^2 \, |V_{tb}|^2 \, \frac{G_F^2}{6\pi^2} \eta_{\rm QCD} m_B B_{B_d} F_{B_d}^2 \times M_W^2 S(x_t) . \quad (33)$$

Using $m_t^\star = 168\,\text{GeV}$ and $\eta_{\rm QCD} = 0.55$ one obtains with the values of Sec. III C

$$0.0069 \leq |V_{td}| \leq 0.0124. \quad (34)$$

This is represented by the shaded band in Fig. 3. One immediately notices, that higher values of $|V_{ub}/V_{cb}|$ and V_{cb} favor the lower branch of the solution, i.e., the smaller solution for δ. While for the central values of our analysis B_d^0-$\overline{B_d^0}$ mixing implies no additional constraint on $|V_{td}|$, we still get a tighter upper bound for $|V_{td}|$ compared to the range (32) implying only $|V_{td}| \leq 0.0130$. From Fig. 4 one can easily verify that varying $m_t^\star$ does not yield a bound on $|V_{td}|$ different from (34) for the combined analysis of ε_K and B_d^0-$\overline{B_d^0}$ mixing. Further note that the band derived from x_d clearly shows δ being different from zero in the whole range of values for $|V_{cb}|$. This is remarkable, because in the standard model the phase δ is responsible for the CP violation and x_d is a quantity having nothing to do with the breakdown of this discrete symmetry.

Let us now explore the $m_t^\star$ dependence of $|V_{td}|$, which is plotted in Fig. 4. The solid curve is identical for (a)–(c) and corresponds to the central values of Sec. III C, we additionally varied in (a) $B_K = 0.65, 0.75, 0.85$, in (b) $V_{cb} = 0.038, 0.040, 0.043$, and in (c) $|V_{ub}/V_{cb}| = 0.07, 0.08, 0.10$. No solution was obtained for (b) $V_{cb} = 0.037$ and (c) $|V_{ub}/V_{cb}| = 0.06$. The band displayed in gray again shows the values allowed for $|V_{td}|$ from x_d. Clearly, for larger values of $m_t^\star$, V_{cb}, and $|V_{ub}/V_{cb}|$ the constraint from x_d favors the lower branch of the solution for $|V_{td}|$.

Figure 4(d) shows the variation of $|V_{td}|$ vs $m_t^\star$ with the value of the strong coupling normalized at M_Z, $\alpha_s(M_Z)$. One notices, that the influence of $\alpha_s(M_Z)$ far off the point where the two solutions merge is quite small. As one expects, the variation of the value m_t at the point where the branches meet is quite large, it amounts to about 6 GeV. This fact was already discussed at the end of Sec. IV.

C. Prediction for Δm_{B_s} and x_s

It is well known (see, e.g., [31]) that an analysis using both x_d and the B_s^0-$\overline{B_s^0}$ mixing parameter x_s allows for a much more precise determination of $|V_{td}|$ than the investigation of x_d alone. The main reason for this is the fact that the hadronic uncertainties in the ratio x_d/x_s are reduced to SU(3) breaking effects and are thereby much smaller than in x_d or x_s alone. Further $|V_{ts}|$ is known very well, because it is related to V_{cb} via the unitarity of the CKM matrix. The present experimental bound on x_s does not constrain the ranges (32) and (34) for $|V_{td}|$ further. Therefore we will instead predict a range for Δm_{B_s} and x_s from our result (32).

We will use the mass difference $\Delta m_{B_q} = x_q/\tau_{B_q}$ with $q = d, s$ in our formulas. From (33) and the analogous formula for x_s one finds

$$\Delta m_{B_s} = \Delta m_{B_d} \frac{|V_{ts}|^2}{|V_{td}|^2} \frac{1}{\widetilde{R}_{ds}} \quad (35)$$

with

$$\widetilde{R}_{ds} = \frac{m_{B_d} F_{B_d}^2 B_{B_d}}{m_{B_s} F_{B_s}^2 B_{B_s}}. \quad (36)$$

$\widetilde{R}_{ds}$ equals 1 in the SU(3) limit. The SU(3) breaking in the decay constants is encoded in (27). Setting

$$\widetilde{R}_{ds} = 0.66 \pm 0.08$$

one gets from (35)

$$\Delta m_{B_s} = (0.76 \pm 0.11)\text{ps}^{-1} \frac{|V_{ts}|^2}{|V_{td}|^2}. \quad (37)$$

Now for $|V_{td}| = 9.3 \times 10^{-3}$ one finds $\Delta m_{B_s} = (13.4 \pm 1.9)\ \text{ps}^{-1}$ corresponding to $x_s = (20.5 \pm 3.2)$ for $\tau_{B_s} = 1.53 \pm 0.10$ [16]. Equivalently $|V_{td}| = 10.6 \times 10^{-3}$ yields $\Delta m_{B_s} = (10.2 \pm 1.5)\ \text{ps}^{-1}$ and $x_s = (15.6 \pm 2.4)$. These values are well above the present lower bound $\Delta m_{B_s} > 6.0\ \text{ps}^{-1}$ from the ALEPH collaboration [32]. In order to find the range for Δm_{B_s} consistent with ε_K and x_d in the parameter range of Sec. III C we use two different methods. First we scan the full range yielding

$$6.3\ \text{ps}^{-1} \leq \Delta m_{B_s} \leq 33\ \text{ps}^{-1},$$

where the error in (37) has been included. Second we restrict the input parameters to the 1σ ellipsoid

$$\left(\frac{|V_{ub}/V_{cb}| - 0.08}{0.02}\right)^2 + \left(\frac{V_{cb} - 0.040}{0.003}\right)^2 + \left(\frac{m_t^\star - 168\,\text{GeV}}{13\,\text{GeV}}\right)^2 + \left(\frac{B_K - 0.75}{0.10}\right)^2 \leq 1, \quad (38)$$

which would be the natural range, if all errors were statistical. Here we find

$$6.8\ \text{ps}^{-1} \leq \Delta m_{B_s} \leq 24\ \text{ps}^{-1}$$

showing that only the upper bound is sensitive to the border region of the parameter space. For our final prediction we use the arithmetic mean of both estimates:

$$6.5\ \text{ps}^{-1} \leq \Delta m_{B_s} \leq 28\ \text{ps}^{-1}. \tag{39}$$

This corresponds to

$$9.3 \leq x_s \leq 46. \tag{40}$$

Future stronger bounds on Δm_{B_s} may be used to rule out the higher solution for $|V_{td}|$ in a part of the parameter space: Since to 1% accuracy $|V_{ts}| = 0.98 V_{cb}$, the relation (37) defines a straight line in Fig. 3 excluding the values for $|V_{td}|$ above this line.

D. Im λ_t

In the discussion of CP violation Im λ_t is of utmost importance. It is proportional to the Jarlskog parameter,

$$2J_{CP} = V_{ud}V_{us}\text{Im}\,\lambda_t = \lambda^6 A^2 \bar{\eta} + O\left(\lambda^8\right), \tag{41}$$

and encodes the same experimental information, because the value of $V_{ud}V_{us}$ is precisely known. For example $\varepsilon'_K/\varepsilon_K$ is proportional to Im λ_t. We tabulate Im λ_t in Table III. Here the lower solution for δ corresponds to the higher value of Im λ_t and vice versa. For our standard choice of parameters from Sec. III C we find

$$\begin{aligned} 10^4 \times \text{Im}\,\lambda_t^{\text{low}} &= 1.15\ {}^{+0.07}_{-0.20}\ {}^{+0.06}_{-0.12}\ {}^{+0.09}_{-0.15}\ {}^{+0.09}_{-0.19}, \\ 10^4 \times \text{Im}\,\lambda_t^{\text{high}} &= 1.28\ {}^{+0.03}_{-0.05}\ {}^{+0.19}_{-0.07}\ {}^{+0.00}_{-0.03}\ {}^{+0.00}_{-0.03}. \end{aligned} \tag{42}$$

The upper line of Im λ_t^{low} and the lower line of Im λ_t^{high} corresponds to $V_{cb,\text{min}}$, $|V_{ub}/V_{cb}|_{\text{min}}$, $m^\star_{t,\text{min}}$, and $B_{K,\text{min}}$ [see the values in the paragraph below (29)], the lower line of Im λ_t^{low} and the upper line of Im λ_t^{high} result from putting the input parameters to their highest allowed value. Note that Im λ_t^{high} is not a monotonous function of the input parameters, for our central values of $m_t^\star$ and B_K we are already close to the maximum.

From the analysis of ε_K alone we find for a scan of the whole parameter range the result

TABLE III. The values for Im λ_t corresponding to the two values of δ in Table I.

$m_t^\star$	B_K	$\left\|\frac{V_{ub}}{V_{cb}}\right\|$	V_{cb} 0.037	0.038	0.039	0.040	0.041	0.042	0.043
						Im$\lambda_t \cdot 10^4$			
155	0.65	0.08	—	—	—	—	—	—	1.47 1.28
155	0.65	0.09	—	—	—	—	1.50 1.42	1.57 1.29	1.59 1.21
155	0.65	0.10	—	—	—	1.60 1.41	1.65 1.30	1.67 1.22	1.68 1.16
155	0.75	0.07	—	—	—	—	—	—	1.28 1.13
155	0.75	0.08	—	—	—	—	1.34 1.22	1.38 1.13	1.38 1.07
155	0.75	0.09	—	—	—	1.43 1.22	1.46 1.14	1.46 1.08	1.46 1.02
155	0.75	0.10	—	—	1.51 1.23	1.53 1.15	1.54 1.09	1.54 1.04	1.53 0.99
155	0.85	0.06	—	—	—	—	—	—	1.11 1.03
155	0.85	0.07	—	—	—	—	1.17 1.10	1.20 1.02	1.20 0.96
155	0.85	0.08	—	—	—	1.27 1.09	1.28 1.02	1.28 0.97	1.27 0.92
155	0.85	0.09	—	1.29 1.21	1.35 1.10	1.36 1.03	1.36 0.98	1.35 0.93	1.34 0.89
155	0.85	0.10	1.37 1.22	1.41 1.12	1.43 1.05	1.43 0.99	1.43 0.95	1.42 0.90	1.40 0.86
168	0.65	0.07	—	—	—	—	—	—	1.29 1.22
168	0.65	0.08	—	—	—	—	—	1.40 1.20	1.42 1.13
168	0.65	0.09	—	—	—	1.43 1.32	1.49 1.21	1.51 1.14	1.51 1.08
168	0.65	0.10	—	—	1.52 1.33	1.57 1.22	1.59 1.15	1.59 1.09	1.59 1.04
168	0.75	0.07	—	—	—	—	—	1.22 1.06	1.23 0.99
168	0.75	0.08	—	—	—	1.28 1.15	1.31 1.06	1.31 1.00	1.30 0.95
168	0.75	0.09	—	—	1.36 1.15	1.38 1.07	1.39 1.01	1.38 0.96	1.37 0.92
168	0.75	0.10	—	1.43 1.17	1.46 1.09	1.46 1.03	1.46 0.98	1.45 0.93	1.44 0.89
168	0.85	0.06	—	—	—	—	—	1.06 0.97	1.06 0.90
168	0.85	0.07	—	—	—	1.12 1.04	1.14 0.96	1.14 0.90	1.13 0.86
168	0.85	0.08	—	—	1.21 1.03	1.22 0.96	1.22 0.91	1.21 0.87	1.19 0.83
168	0.85	0.09	1.22 1.15	1.28 1.04	1.29 0.98	1.29 0.92	1.28 0.88	1.27 0.84	1.25 0.80
168	0.85	0.10	1.34 1.06	1.36 0.99	1.36 0.94	1.36 0.89	1.35 0.85	1.33 0.81	1.31 0.78
181	0.65	0.07	—	—	—	—	—	1.23 1.16	1.26 1.06
181	0.65	0.08	—	—	—	—	1.34 1.14	1.35 1.07	1.35 1.01
181	0.65	0.09	—	—	1.36 1.27	1.42 1.15	1.43 1.08	1.44 1.02	1.43 0.97
181	0.65	0.10	—	1.44 1.27	1.49 1.17	1.51 1.09	1.52 1.03	1.51 0.98	1.50 0.94
181	0.75	0.06	—	—	—	—	—	—	1.09 0.94
181	0.75	0.07	—	—	—	—	1.16 1.00	1.17 0.94	1.16 0.89
181	0.75	0.08	—	—	1.22 1.09	1.24 1.01	1.25 0.95	1.24 0.90	1.23 0.86
181	0.75	0.09	—	1.29 1.10	1.32 1.02	1.32 0.96	1.32 0.91	1.31 0.87	1.29 0.83
181	0.75	0.10	1.36 1.12	1.39 1.04	1.40 0.98	1.39 0.93	1.39 0.88	1.37 0.84	1.36 0.80
181	0.85	0.06	—	—	—	—	1.01 0.92	1.01 0.85	1.00 0.81
181	0.85	0.07	—	—	1.06 0.99	1.09 0.91	1.09 0.86	1.08 0.81	1.06 0.77
181	0.85	0.08	—	1.15 0.99	1.16 0.92	1.16 0.87	1.15 0.82	1.14 0.78	1.12 0.75
181	0.85	0.09	1.22 1.00	1.23 0.93	1.23 0.88	1.22 0.83	1.21 0.79	1.19 0.76	1.17 0.73
181	0.85	0.10	1.30 0.95	1.30 0.90	1.29 0.85	1.28 0.81	1.27 0.77	1.25 0.74	1.23 0.71

$$0.71 \times 10^{-4} \leq \mathrm{Im}\,\lambda_t \leq 1.68 \times 10^{-4}. \quad (43)$$

Next we include the constraint from x_d: We now find the lower bound in the full parameter range in (43) shifted from 0.71 to 0.81. For the parameter range (38) we find

$$0.89 \times 10^{-4} \leq \mathrm{Im}\,\lambda_t \leq 1.51 \times 10^{-4}. \quad (44)$$

We combine the two estimates to our final result

$$0.85 \times 10^{-4} \leq \mathrm{Im}\,\lambda_t \leq 1.60 \times 10^{-4}. \quad (45)$$

The $m_t^\star$ dependence of $\mathrm{Im}\,\lambda_t$ may be looked at in Fig. 5. Plot (a) shows this dependence for three values of $|V_{cb}|$, plot (b) uses four values for $|V_{ub}/V_{cb}|$. Note that the result for $\mathrm{Im}\,\lambda_t$ on the upper branch is essentially independent of V_{cb}, whereas the lower branch varies quite strongly with V_{cb}.

E. $\bar{\rho}$, $\bar{\eta}$ and the unitarity triangle

Our knowledge about the CKM parameters related to CP violation is usually expressed by the unitarity triangle introduced in Sec. III A.

Using δ from Table I, one obtains the allowed pairs of $(\bar{\rho}, \bar{\eta})$ listed in the Tables IV and V. Note that this table is constructed solely from the unitarity of the CKM ma-

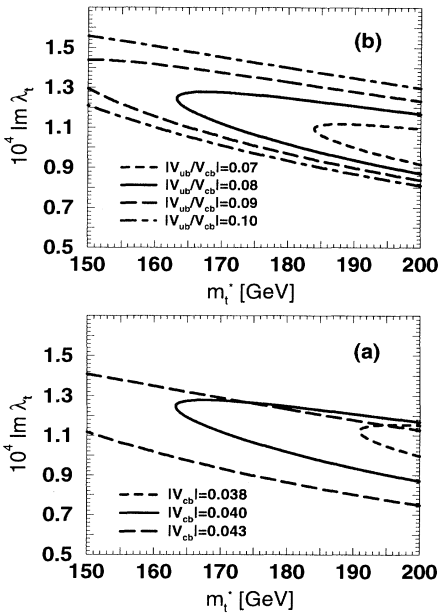

FIG. 5. The dependence of $\mathrm{Im}\,\lambda_t$ on $m_t^\star$ for (a) three values of $|V_{cb}|$ and (b) four values of $|V_{ub}/V_{cb}|$. In plot (a) one observes that the higher solution for $\mathrm{Im}\,\lambda_t$ is stable with respect to the variation of $|V_{cb}|$, whereas the lower branch depends quite strongly on this parameter.

TABLE IV. The values for $\bar{\rho}$ corresponding to the two values of δ in Table I.

		V_{cb}	0.037	0.038	0.039	0.040	0.041	0.042	0.043
$m_t^\star$	B_K	$\lvert\frac{V_{ub}}{V_{cb}}\rvert$				$\bar{\rho}$			
155	0.65	0.08	—	—	—	—	—	—	0.026 -0.175
155	0.65	0.09	—	—	—	—	-0.055 -0.139	0.060 -0.232	0.120 -0.273
155	0.65	0.10	—	—	—	-0.015 -0.208	0.081 -0.279	0.141 -0.318	0.186 -0.344
155	0.75	0.07	—	—	—	—	—	—	0.035 -0.151
155	0.75	0.08	—	—	—	—	-0.002 -0.149	0.078 -0.212	0.127 -0.245
155	0.75	0.09	—	—	—	0.036 -0.211	0.106 -0.262	0.155 -0.292	0.192 -0.313
155	0.75	0.10	—	—	0.055 -0.258	0.125 -0.306	0.176 -0.336	0.215 -0.357	0.247 -0.373
155	0.85	0.06	—	—	—	—	—	—	0.006 -0.097
155	0.85	0.07	—	—	—	—	-0.014 -0.107	0.068 -0.175	0.113 -0.207
155	0.85	0.08	—	—	—	0.043 -0.184	0.105 -0.229	0.148 -0.257	0.180 -0.276
155	0.85	0.09	—	-0.041 -0.145	0.072 -0.236	0.132 -0.276	0.175 -0.303	0.209 -0.322	0.237 -0.336
155	0.85	0.10	-0.014 -0.202	0.088 -0.279	0.151 -0.319	0.197 -0.346	0.233 -0.365	0.263 -0.379	0.288 -0.391
168	0.65	0.07	—	—	—	—	—	—	-0.028 -0.099
168	0.65	0.08	—	—	—	—	—	0.036 -0.184	0.098 -0.229
168	0.65	0.09	—	—	—	-0.039 -0.155	0.067 -0.239	0.125 -0.278	0.168 -0.303
168	0.65	0.10	—	—	-0.011 -0.214	0.084 -0.284	0.145 -0.322	0.190 -0.347	0.226 -0.366
168	0.75	0.07	—	—	—	—	—	0.044 -0.159	0.097 -0.198
168	0.75	0.08	—	—	—	0.005 -0.157	0.083 -0.217	0.131 -0.249	0.167 -0.271
168	0.75	0.09	—	—	0.038 -0.215	0.109 -0.265	0.158 -0.295	0.195 -0.316	0.225 -0.332
168	0.75	0.10	—	0.054 -0.260	0.126 -0.308	0.177 -0.338	0.217 -0.360	0.250 -0.375	0.277 -0.388
168	0.85	0.06	—	—	—	—	—	0.018 -0.108	0.075 -0.154
168	0.85	0.07	—	—	—	-0.005 -0.116	0.073 -0.179	0.118 -0.211	0.150 -0.231
168	0.85	0.08	—	—	0.045 -0.187	0.108 -0.232	0.151 -0.260	0.183 -0.279	0.209 -0.293
168	0.85	0.09	-0.049 -0.141	0.071 -0.237	0.132 -0.278	0.177 -0.305	0.211 -0.324	0.239 -0.338	0.262 -0.349
168	0.85	0.10	0.085 -0.279	0.149 -0.320	0.197 -0.347	0.234 -0.367	0.265 -0.381	0.290 -0.392	0.311 -0.401
181	0.65	0.07	—	—	—	—	—	-0.019 -0.109	0.064 -0.177
181	0.65	0.08	—	—	—	—	0.038 -0.187	0.100 -0.231	0.143 -0.259
181	0.65	0.09	—	—	-0.047 -0.150	0.065 -0.239	0.126 -0.279	0.169 -0.305	0.204 -0.323
181	0.65	0.10	—	-0.021 -0.208	0.081 -0.283	0.143 -0.322	0.190 -0.348	0.227 -0.367	0.257 -0.381
181	0.75	0.06	—	—	—	—	—	—	0.053 -0.139
181	0.75	0.07	—	—	—	—	0.045 -0.161	0.099 -0.200	0.136 -0.224
181	0.75	0.08	—	—	0.000 -0.155	0.082 -0.217	0.131 -0.250	0.168 -0.272	0.197 -0.288
181	0.75	0.09	—	0.031 -0.212	0.106 -0.264	0.156 -0.296	0.195 -0.317	0.225 -0.333	0.250 -0.345
181	0.75	0.10	0.043 -0.255	0.120 -0.306	0.174 -0.338	0.216 -0.360	0.249 -0.376	0.277 -0.388	0.300 -0.398
181	0.85	0.06	—	—	—	—	0.019 -0.110	0.077 -0.156	0.112 -0.181
181	0.85	0.07	—	—	-0.011 -0.113	0.072 -0.180	0.118 -0.212	0.151 -0.232	0.176 -0.248
181	0.85	0.08	—	0.038 -0.184	0.105 -0.232	0.149 -0.260	0.183 -0.279	0.210 -0.294	0.231 -0.305
181	0.85	0.09	0.062 -0.233	0.128 -0.277	0.174 -0.304	0.210 -0.324	0.239 -0.338	0.262 -0.349	0.282 -0.358
181	0.85	0.10	0.142 -0.318	0.193 -0.346	0.232 -0.366	0.263 -0.381	0.289 -0.393	0.311 -0.402	0.329 -0.409

TABLE V. The values for $\bar{\eta}$ corresponding to the two values of δ in Table I.

V_{cb}			0.037	0.038	0.039	0.040	0.041	0.042	0.043
$m_t^\star$	B_K	$\left\|\frac{V_{ub}}{V_{cb}}\right\|$				$\bar{\eta}$			
155	0.65	0.08	—	—	—	—	—	—	0.352 0.307
155	0.65	0.09	—	—	—	—	0.394 0.373	0.393 0.323	0.379 0.290
155	0.65	0.10	—	—	—	0.441 0.390	0.434 0.342	0.419 0.307	0.400 0.278
155	0.75	0.07	—	—	—	—	—	—	0.307 0.270
155	0.75	0.08	—	—	—	—	0.353 0.320	0.345 0.283	0.330 0.255
155	0.75	0.09	—	—	—	0.396 0.337	0.383 0.299	0.366 0.270	0.348 0.245
155	0.75	0.10	—	—	0.438 0.358	0.423 0.319	0.405 0.287	0.385 0.260	0.366 0.237
155	0.85	0.06	—	—	—	—	—	—	0.265 0.247
155	0.85	0.07	—	—	—	—	0.309 0.290	0.301 0.255	0.288 0.230
155	0.85	0.08	—	—	—	0.351 0.302	0.337 0.269	0.321 0.243	0.304 0.221
155	0.85	0.09	—	0.395 0.370	0.391 0.320	0.375 0.286	0.357 0.258	0.338 0.234	0.319 0.213
155	0.85	0.10	0.441 0.393	0.433 0.342	0.415 0.305	0.395 0.275	0.375 0.249	0.354 0.227	0.335 0.207
168	0.65	0.07	—	—	—	—	—	—	0.308 0.293
168	0.65	0.08	—	—	—	—	—	0.351 0.301	0.339 0.269
168	0.65	0.09	—	—	—	0.396 0.366	0.392 0.318	0.377 0.285	0.360 0.258
168	0.65	0.10	—	—	0.442 0.386	0.433 0.339	0.417 0.303	0.399 0.274	0.379 0.249
168	0.75	0.07	—	—	—	—	—	0.306 0.265	0.293 0.238
168	0.75	0.08	—	—	—	0.353 0.317	0.343 0.279	0.328 0.251	0.311 0.227
168	0.75	0.09	—	—	0.396 0.334	0.382 0.296	0.365 0.266	0.346 0.241	0.328 0.219
168	0.75	0.10	—	0.438 0.357	0.423 0.317	0.404 0.284	0.384 0.257	0.364 0.233	0.344 0.213
168	0.85	0.06	—	—	—	—	—	0.264 0.242	0.254 0.216
168	0.85	0.07	—	—	—	0.309 0.287	0.300 0.252	0.286 0.227	0.270 0.205
168	0.85	0.08	—	—	0.350 0.300	0.336 0.266	0.320 0.240	0.302 0.217	0.285 0.198
168	0.85	0.09	0.394 0.372	0.391 0.319	0.375 0.284	0.356 0.255	0.337 0.231	0.317 0.210	0.299 0.192
168	0.85	0.10	0.433 0.343	0.416 0.304	0.395 0.273	0.374 0.247	0.353 0.224	0.333 0.204	0.314 0.186
181	0.65	0.07	—	—	—	—	—	0.309 0.290	0.302 0.254
181	0.65	0.08	—	—	—	—	0.351 0.300	0.339 0.267	0.323 0.241
181	0.65	0.09	—	—	0.395 0.368	0.392 0.318	0.377 0.283	0.359 0.256	0.341 0.232
181	0.65	0.10	—	0.441 0.390	0.434 0.339	0.418 0.302	0.399 0.272	0.379 0.247	0.359 0.224
181	0.75	0.06	—	—	—	—	—	—	0.260 0.225
181	0.75	0.07	—	—	—	—	0.306 0.264	0.293 0.236	0.278 0.213
181	0.75	0.08	—	—	0.353 0.318	0.344 0.279	0.328 0.250	0.311 0.226	0.293 0.205
181	0.75	0.09	—	0.396 0.337	0.383 0.297	0.365 0.266	0.346 0.240	0.327 0.218	0.308 0.198
181	0.75	0.10	0.439 0.361	0.425 0.318	0.406 0.285	0.385 0.256	0.364 0.232	0.344 0.211	0.324 0.193
181	0.85	0.06	—	—	—	—	0.264 0.241	0.254 0.214	0.240 0.193
181	0.85	0.07	—	—	0.309 0.288	0.301 0.252	0.286 0.226	0.270 0.204	0.254 0.185
181	0.85	0.08	—	0.351 0.302	0.337 0.267	0.320 0.240	0.302 0.216	0.284 0.197	0.267 0.179
181	0.85	0.09	0.393 0.322	0.376 0.285	0.357 0.256	0.337 0.231	0.318 0.209	0.299 0.190	0.280 0.174
181	0.85	0.10	0.418 0.307	0.397 0.274	0.376 0.247	0.354 0.223	0.334 0.203	0.314 0.185	0.294 0.169

trix and the constraint from $|\varepsilon_K|$. The additional constraint from x_d can be included by recalling from (13) that

$$(1-\bar{\rho})^2+\bar{\eta}^2=\left|\frac{V_{td}V_{tb}}{V_{cd}V_{cb}}\right|^2. \tag{46}$$

Since to 0.2% accuracy $|V_{cd}|=V_{us}=0.22$ and $|V_{tb}|=1$ the determination of $|V_{td}|$ from (33) yields a circle in the $\bar{\rho}$-$\bar{\eta}$ plane around $(1,0)$ for each pair $(m_t^\star, V_{cb})$.

In Fig. 6 we display the allowed region for the pair $(\bar{\rho},\bar{\eta})$ including the constraint from x_d (33) described in Sec. V B. Applying this constraint results in cutting the allowed region of $(\bar{\rho},\bar{\eta})$ on the left side of the figure. To obtain a reasonable estimate of the error present in the analysis, we have again used two methods. The area displayed in dark gray results from varying the input parameters B_K, $m_t^\star$, V_{cb}, $|V_{ub}/V_{cb}|$ in the full parameter range described in Sec. III C, the area displayed in light gray is obtained by requiring the used parameters to lie within the four-dimensional 1σ ellipsoid described in (38).

From Fig. 6 we read off the following allowed regions for $(\bar{\rho},\bar{\eta})$ and the angles α, β, γ in Fig. 1:

$$\begin{aligned} -0.37 \le \bar{\rho} \le 0.33\ , \quad & -0.34 \le \bar{\rho} \le 0.23\ , \\ 0.19 \le \bar{\eta} \le 0.44\ , \quad & 0.22 \le \bar{\eta} \le 0.43\ , \\ 22.3^\circ \le \alpha \le 114.3^\circ\ , \quad & 26.2^\circ \le \alpha \le 102.1^\circ\ , \\ 9.1^\circ \le \beta \le 26.2^\circ\ , \quad & 14.9^\circ \le \beta \le 26.2^\circ\ , \\ 42.0^\circ \le \gamma \le 148.2^\circ\ , \quad & 55.5^\circ \le \gamma \le 143.3^\circ\ . \end{aligned} \tag{47}$$

The ranges quoted in the first column correspond to the error estimate by the box scan, the second column to the 1σ-ellipsoid method. Again we quote as our final range the arithmetic mean of both estimates:

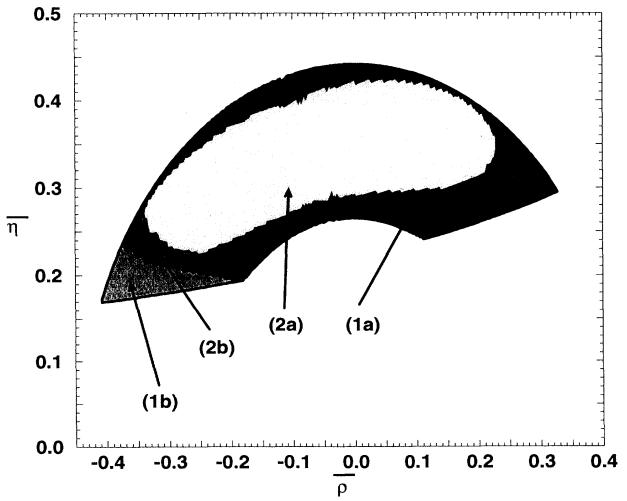

FIG. 6. The allowed region for the pair $(\bar{\rho},\bar{\eta})$ consistent with ε_K and x_d. Area (1a) is obtained from a scan over the full parameter range of Sec. III C. Region (2a) corresponds to the parameters in the 1σ ellipsoid (38). Areas (1b) and (2b) are consistent with ε_K, but not with x_d.

$$\begin{aligned} -0.36 \le \bar{\rho} \le 0.28\ , \\ 0.21 \le \bar{\eta} \le 0.44\ , \\ 24^\circ \le \alpha \le 108^\circ\ , \\ 12^\circ \le \beta \le 26^\circ\ , \\ 49^\circ \le \gamma \le 146^\circ\ . \end{aligned} \tag{48}$$

CP asymmetries in the B system are proportional to the sines of 2α, 2β, or 2γ. We can only reliably predict $\sin 2\beta$:

$$0.41 \le \sin 2\beta \le 0.79,$$

where the upper bound stems solely from $|V_{ub}/V_{cb}| \le 0.10$ (see [10]).

Since to 0.1% accuracy $\delta = \gamma$ we can now improve the range (30) by the inclusion of the constraint from x_d:

$$49^\circ \le \delta \le 146^\circ.$$

VI. A 1995 LOOK AT THE K_L-K_S MASS DIFFERENCE

In this section we will have a look at the status of the K_L-K_S mass difference Δm_K. The short distance part of Δm_K, denoted by $(\Delta m_K)_{\rm SD}$, reads

$$\frac{(\Delta m_K)_{\rm SD}}{m_K} = \frac{G_F^2}{6\pi^2} f_K^2 B_K M_W^2 \left[(\mathrm{Re}\,\lambda_c)^2\, x_c^\star \eta_1^\star + 2\,(\mathrm{Re}\,\lambda_c)\,(\mathrm{Re}\,\lambda_t)\, S\,(x_c^\star, x_t^\star)\, \eta_3^\star + (\mathrm{Re}\,\lambda_t)^2\, S\,(x_t^\star)\, \eta_2^\star \right], \tag{49}$$

where the small imaginary parts of λ_c and λ_t have been neglected. The three terms in the brackets contribute roughly in the ratio 100:10:1, therefore the term containing $\eta_1^\star$ is most important, the one with $\eta_2^\star$ is least.

Because $\eta_1^\star$ strongly depends on its input parameters, especially on $m_c^\star$ and $\Lambda_{\overline{MS}}^{\rm NLO}$, it does not make sense to use the constant defined in (7). We therefore calculate $\eta_1^\star$ for each set of parameters in our numerical evaluation. Inserting our standard set of values defined in Sec. III C, we obtain

$$\frac{(\Delta m_K)_{\rm SD}}{(\Delta m_K)_{\rm exp}} = \begin{cases} 0.52\ ^{+0.17}_{-0.11}\ , & \text{for} \quad \Lambda_{\overline{MS}}^{\rm NLO} = 0.210\,\text{GeV} \\ 0.67\ ^{+0.25}_{-0.14}\ , & \text{for} \quad \Lambda_{\overline{MS}}^{\rm NLO} = 0.310\,\text{GeV} \\ 0.91\ ^{+0.39}_{-0.20}\ , & \text{for} \quad \Lambda_{\overline{MS}}^{\rm NLO} = 0.410\,\text{GeV}\ . \end{cases} \tag{50}$$

The errors are estimated by a scan through the allowed parameter space and includes the error stemming from scale variations in the $\eta_i^\star$'s.

The strong $\Lambda_{\overline{MS}}^{\rm NLO}$ dependence of $(\Delta m_K)_{\rm SD}\,/\,(\Delta m_K)_{\rm exp}$ has been visualized in Fig. 7. The central line is obtained by using the central values defined in Sec. III C, the band shaded in gray displays the error.

For large values of $\Lambda_{\overline{MS}}^{\rm NLO}$ the uncertainties in $\eta_1^\star$ due to scale variations become large indicating the breakdown of perturbation theory. Therefore the error bar on Δm_K which is then dominated by this scale uncertainty grows very large prohibiting a precise prediction for the mass difference. One will have to see, whether in the future $\Lambda_{\overline{MS}}^{\rm NLO}$ will continue growing in the future and thereby bringing the next-to-leading order result for $\eta_1^\star$ into troubles.

Let us now discuss the differences between our new result and previous analyses: In most textbooks Δm_K is termed to be dominated by poorly calculable long distance physics. Yet by power counting arguments, long distance effects should be suppressed by a power of $\Lambda_{\rm QCD}^2/m_c^{\star\,2}$ with respect to the short distance part because the coefficient of the leading dimension six operator contributing to the $\eta_1^\star$ part of the effective Hamiltonian in (3) is proportional to $m_c^{\star\,2}$ (see, e.g., [33]).

A short look at (50) clearly exhibits a short distance dominance. Let us discuss the steps which have guided

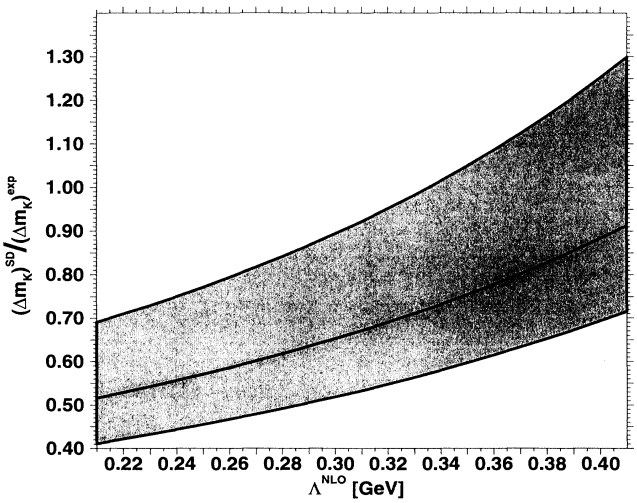

FIG. 7. The dependence of the ratio of the short distance part of the K_L-K_S mass difference to the experimentally measured value on $\Lambda^{\rm NLO} \equiv \Lambda_{\overline{MS}}^{\rm NLO}$. The curve in the middle is obtained by choosing the central values of the parameters as given in Sec. III C. All values lying in the shaded area are compatible within the error bands quoted in this section. The increasing height of the band displaying the error is due to the growing scale uncertainties present in the coefficient $\eta_1^\star$.

us to this result.

Already our 1993 analysis [6], in which we have calculated the coefficient $\eta_1^\star$ in the next-to-leading order approximation, has resulted in a large enhancement of the theoretical prediction for the K_L-K_S mass difference. This fact is true, because

(i) the next-to-leading order correction has largely increased the value of $\eta_1^\star$ and

(ii) the experimental value for $\Lambda_{\overline{MS}}^{\rm NLO}$ has risen in the last decade.

Both findings lead to the drastic increase of $\eta_1^\star$ by approximately 65%, which we get by comparing (8) and (7).

Finally, our new analysis compared to [6] for the first time uses the coefficient $\eta_3^\star$ calculated in the next-to-leading approximation. This quantity again enlarges the result for Δm_K. Because $\Lambda_{\overline{MS}}^{\rm NLO}$ has grown again in the meantime thereby enlarging the theoretical prediction once more, we are now able to reproduce the experimentally measured value to 50–100 % by short distance physics.

Some authors attributed the deficit in Δm_K to new physics. The large-scale uncertainties present in the coefficient $\eta_1^\star$, which obscure a clean determination of the standard model contribution, make the K_L-K_S mass difference a poor laboratory to search for the impact of new physics.

ACKNOWLEDGMENTS

We thank Andrzej Buras for suggesting the topic and constant encouragement. We have enjoyed many useful discussions with him and Gaby Ostermaier. U.N. thanks Patricia Ball for her explanations of the determination of V_{cb} in [13] and Ikarus Bigi for discussions on the same topic. S.H. thanks Fred Jegerlehner for interesting discussions. This work was supported by BMBF under Contract No. 06-TM-743.

[1] J. H. Christenson, J. W. Cronin, V. L. Fitch, and R. Turlay, Phys. Rev. Lett. **13**, 138 (1964); J. H. Christenson, J. W. Cronin, V. L. Fitch, and R. Turlay, Phys. Rev. **140**, B74 (1965).

[2] L. Chau, Phys. Rep. **95**, 1 (1983); A. J. Buras and M. K. Harlander, *A Top-Quark Story: Quark Mixing, CP-Violation and Rare Decays in the Standard Model*, in *Heavy Flavours*, edited by A. J. Buras and M. Lindner (World Scientific, Singapore, 1993).

[3] T. Inami and C. S. Lim, Prog. Theor. Phys. **65**, 297 (1981); **65** 1772(E) (1981).

[4] F. J. Gilman and M. B. Wise, Phys. Rev. D **27**, 1128 (1983).

[5] J. M. Flynn, Mod. Phys. Lett. A **5**, 877 (1990); A. Datta, J. Fröhlich, and E. A. Paschos, Z. Phys. C **46**, 63 (1990).

[6] S. Herrlich and U. Nierste, Nucl. Phys. **B419**, 292 (1994).

[7] A. J. Buras, M. Jamin, and P. H. Weisz, Nucl. Phys. **B347**, 491 (1990).

[8] S. Herrlich and U. Nierste, "The complete $|\Delta S| = 2$ Hamiltonian in next-to-leading order," Technische Universität München Report No. TUM-T31-86/95 (unpublished); U. Nierste, "Indirect CP violation in the neutral kaon system and related topics," thesis TU München, 1995, hep-ph/9510323 (unpublished).

[9] Particle Data Group, L. Montanet *et al.*, Phys. Rev. D **50**, 1173 (1994).

[10] A. J. Buras, M. E. Lautenbacher, and G. Ostermaier, Phys. Rev. D **50**, 3433 (1994).

[11] L. Wolfenstein, Phys. Rev. Lett. **51**, 1945 (1983).

[12] A. J. Buras, M. Jamin, and P. H. Weisz, Nucl. Phys. **B408**, 209 (1993).

[13] P. Ball, M. Beneke, and V. M. Braun, Phys. Rev. D **52**, 3929 (1995).

[14] I. Bigi, Plenary talk at the DPG conference, Karls-
ruhe, 1995.

[15] P. Ball and U. Nierste, Phys. Rev. D **50**, 5841 (1994).

[16] O. Podobrin, Plenary talk at the DPG conference, Karlsruhe, 1995.

[17] CDF Collaboration, F. Abe *et al.*, Phys. Rev. D **50**, 2966 (1994); Phys. Rev. Lett. **73**, 225 (1994).

[18] S. Riemann, Plenary talk at the DPG conference, Karlsruhe, 1995.

[19] D0 Collaboration, S. Abachi *et al.*, Phys. Rev. Lett. **74**, 2632 (1995).

[20] D. E. Soper, *Summary of the XXX Recontre de Moriond, QCD Session*, hep-ph/9506218 (unpublished).

[21] W. A. Bardeen, A. J. Buras, and J.-M. Gérard, Phys. Lett. B **211**, 343 (1988); J.-M. Gérard, Acta Phys. Pol. B **21**, 257 (1990).

[22] J. F. Donoghue, E. Golowich, and B. R. Holstein, Phys. Lett. B **119**, 412 (1982).

[23] A. Pich and E. de Rafael, Phys. Lett. B **158**, 477 (1985); J. Prades *et al.*, Z. Phys. C **51**, 287 (1991).

[24] J. Bijnens and J. Prades, Nucl. Phys. **B444**, 523 (1995).

[25] M. Crisafulli *et al.*, in *Lattice '94*, Proceedings of the International Symposium, Bielefeld, Germany, 1994, edited by F. Karsch, J. Engels, E. Haermann, and B. Petersson [Nucl. Phys. B (Proc. Suppl.) **42** (1995)].

[26] N. Ishizuka *et al.*, Phys. Rev. Lett. **71** , 24 (1993).

[27] S. Bethke, Proceedings of the Summer School on Hadronic Aspects of Collider Physics, Zuoz, Switzerland, 1994 (unpublished).

[28] A. Duncan, E. Eichten, J. Flynn, B. Hill, G. Hockney, and H. Thacker, Phys. Rev. D **51**, 5101 (1995); C. W. Bernard, J. N. Labrenz, and A. Soni, *ibid.* **49**, 2536 (1994); T. Draper and C. McNeile, Nucl. Phys. (Proc. Suppl.) **34**, 453 (1994).

[29] E. Bagan, P. Ball, V. M. Braun, and H. G. Dosch, Phys. Lett. B **278**, 457 (1992); M. Neubert, Phys. Rev. D **45**, 2451 (1992).

[30] A. J. Buras, Phys. Lett. B **317**, 449 (1993).

[31] A. Ali and D. London, *Proceedings of ECFA Workshop on the Physics of a B Meson Factory, 1993*, edited by R. Aleksan and A. Ali [DESY Report No. DESY-93-022 (unpublished)].

[32] K. Jakobs, ALEPH, Talk at the DPG conference, Karlsruhe, 1995.

[33] M. A. Shifman, Int. J. Mod. Phys. A **12**, 2769 (1988).

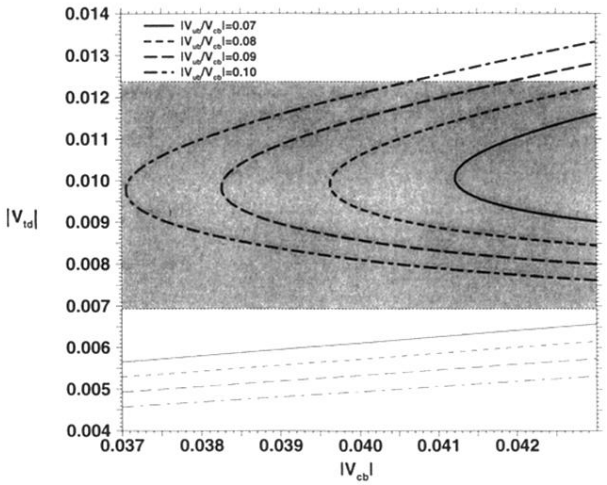

FIG. 3. The dependence of $|V_{td}|$ on V_{cb} for $B_K = 0.75$, $m_t^* = 168\,\mathrm{GeV}$, and four values of $|V_{ub}/V_{cb}|$. The thin lines correspond to $\delta = 0$, i.e., no CP violation. The shaded area is consistent with x_d from (34).

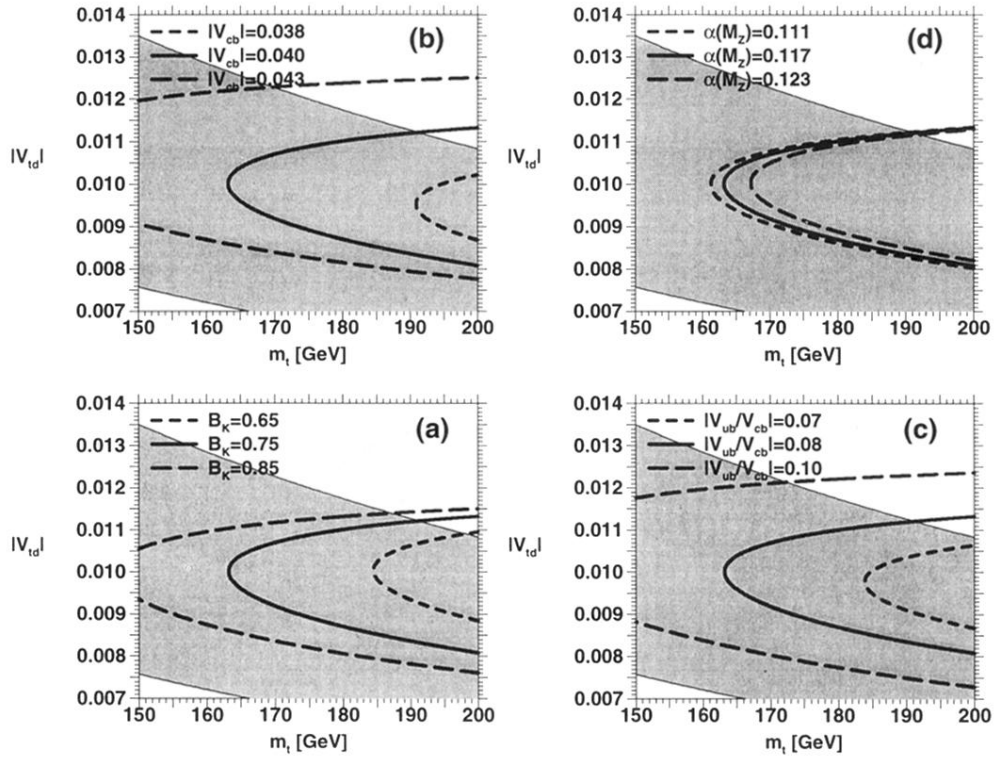

FIG. 4. The dependence of $|V_{td}|$ on $m_t^\star$ for three values of (a) B_K, (b) V_{cb}, (c) $|V_{ub}/V_{cb}|$, and (d) $\alpha(M_Z)$. All other parameters equal their central values of Sec. III C. The shaded area gives the band (34) of $|V_{td}|$'s allowed by the B_d^0-$\overline{B_d^0}$ mixing parameter x_d. For large values of the discussed parameters x_d favors the smaller branch of the solution.

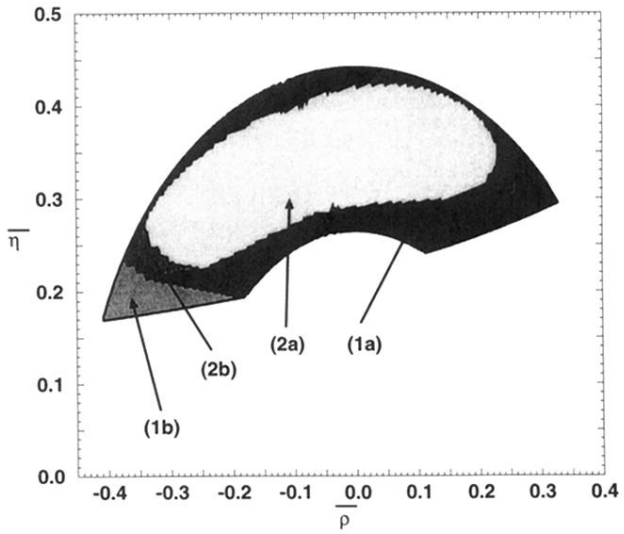

FIG. 6. The allowed region for the pair $(\bar{\rho}, \bar{\eta})$ consistent with ε_K and x_d. Area (1a) is obtained from a scan over the full parameter range of Sec. III C. Region (2a) corresponds to the parameters in the 1σ ellipsoid (38). Areas (1b) and (2b) are consistent with ε_K, but not with x_d.

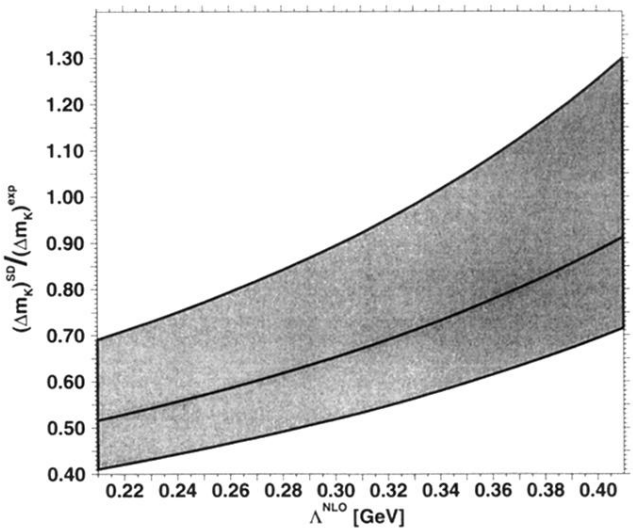

FIG. 7. The dependence of the ratio of the short distance part of the K_L-K_S mass difference to the experimentally measured value on $\Lambda^{\rm NLO} \equiv \Lambda^{\rm NLO}_{\overline{MS}}$. The curve in the middle is obtained by choosing the central values of the parameters as given in Sec. III C. All values lying in the shaded area are compatible within the error bands quoted in this section. The increasing height of the band displaying the error is due to the growing scale uncertainties present in the coefficient $\eta_1^\star$.